INTERNATIONAL JOURNAL OF NUMERICAL MODELLING: ELECTRONIC NETWORKS, DEVICES AND FIELDS
Int. J. Numer. Model. 2012; **25**:441–453
Published online 16 April 2012 in Wiley Online Library (wileyonlinelibrary.com). DOI: 10.1002/jnm.1839

An improved truly meshless method based on a new shape function and nodal integration

Hooman Razmjoo, Masoud Movahhedi*,† and Ahmad Hakimi

Department of Electrical Engineering, Shahid Bahonar University of Kerman, Kerman, Iran

SUMMARY

An improved truly meshless method is presented for three-dimensional (3D) electromagnetic problems. In the proposed method, the computational time for the construction of the introduced shape function is lower than the other meshless methods considerably. An efficient and stable nodal integration technique based on the Taylor series extension is also used in the proposed meshless method. Weak-form formulations adopted for creating discretized system equations of electrostatic and electromagnetic 3D problems are also presented. In the proposed fast truly meshless method, unlike in traditional meshless schemes where background mesh is utilized to compute integrals, nodal integration is used to avoid meshing. The numerical solutions for electrostatic and electromagnetic problems show that the presented method is a robust meshfree method and possesses better computational properties compared with traditional meshless methods. Copyright © 2012 John Wiley & Sons, Ltd.

Received 5 August 2011; Revised 17 January 2012; Accepted 27 February 2012

KEY WORDS: meshless (meshfree) methods; nodal integration; shape function; electrostatic; electromagnetics

1. INTRODUCTION

Meshless or meshfree methods in computational mechanics have attracted much attention in recent decades. They can also be used to solve many engineering problems in different fields that do not lend themselves to solutions by using such traditional methods as the FEM or the BEM, especially extremely large deformation problems. The main objective of meshless methods is to get rid of, or at least to alleviate, the complexity of meshing and remeshing the entire structure domain by simply adding or deleting nodes.

There are several types of meshfree methods, in which the main difference between them is in the way the shape function is constructed. But the most widely employed meshless methods are the following: the element-free Galerkin (EFG) method (which was developed by Belytschko *et al*. [1]), the smooth particle hydrodynamics (which depends only on a set of disordered points or particles and has enjoyed considerable popularity in computational physics [2]), the partition of unity method (PUM) [3,4], the natural element method [5], the point interpolation method [6] (which is a subclass of the so-called PUM [7]), and finally, the recently proposed meshless method based on a new shape function [8–10] (which can save considerable amount of simulation time in time-domain and frequency-domain electromagnetic problems).

In all of these meshless methods, shape functions will be constructed without any mesh information. But to evaluate the integrals appearing in their weak-form formulations, a background mesh is required, which adumbrates methods to being truly meshfree. To eliminate this drawback, some truly meshless methods that rely on nodal integration techniques have been proposed. Beissel and Belytschko [11] used nodal integration to eliminate the background mesh in the EFG method. In [12], the nodal integration technique applied to the meshless formulation based on the radial point

*Correspondence to: Masoud Movahhedi, Department of Electrical Engineering, Shahid Bahonar University of Kerman, Kerman, Iran.
†E-mail: movahhedi@ieee.org

interpolation method (RPIM) has been used and is expanded up to the second order. But the nodal integration technique in meshless methods sometimes causes some undesired oscillations in the results, which can be reduced by adding some stabilization terms to the weak-form formulation. To resolve this disadvantage, Chen *et al.* [13] introduced a stabilized conforming nodal integration technique. Moreover, Rosca and Leitao [14] efficiently used the Monte Carlo integration technique in meshless methods based on global and local weak forms. They implemented this technique for the EFG method and the meshless local Petrov–Galerkin method. Also, the Taylor series expansion can be used for other truly meshfree methods [15]. The proposed formulation is based on the EFG method that uses moving least squares (MLS) shape functions, and the first-order Taylor series expansion to the strain matrix is employed for stabilization [15].

As mentioned previously, some nodal integration techniques have been proposed for the integration of weak-form formulation in meshless methods. In this work, we attempt to examine an alternative, stable, and simple nodal integration technique for meshfree weak-form methods when it is implemented in the process of numerical integration for the novel shape function proposed in [8]. In this case, the formulation is based on a new approach described in [8] to solve three-dimensional electromagnetic problems. To do this, third-order derivatives of shape functions are required for potential and wave equations.

Most conventional meshless methods (e.g., MLS and RPIM) need to compute the inversion of a matrix, which is usually an expensive process, to obtain shape functions. But in the proposed procedure, which has been introduced in [8] and is described and extended to three-dimensional problems in the following paper, there is no need to do that. In the proposed method, shape functions would be constructed directly and therefore faster. Moreover, it is verified that by doing some modifications on the shape functions, we can reach acceptable accuracy in the results for different time-domain and frequency-domain electromagnetic problems [7–10]. In this paper, we employ this approach to construct three-dimensional shape functions. Moreover, to achieve a truly meshless method, a nodal integration technique is used to evaluate meshless weak-form integrals and to solve three-dimensional electrostatic and electromagnetic problems.

The outline of this paper is as follows. In Section 2, the procedure leading to a fast meshless scheme is briefly introduced. In Section 3, basic equations including the meshless weak form for scalar potential equation are briefly discussed. In Section 4, an efficient nodal integration technique based on the Taylor series expansion is presented for three-dimensional problems. In Section 5, three-dimensional numerical examples are examined to study the accuracy and the efficiency of the present fast meshless method in electrostatic and electromagnetic problems. Finally, in Section 6, we provide conclusions for this work.

2. FAST MESHLESS APPROACH

This section focuses on a great challenge in meshless methods, that is, the shape function construction. According to the data-fitting algorithm and the PUM, a complete approach for constructing shape functions has been proposed, and its performance in electromagnetic problems in different situations has been investigated [8,9]. A new weighting function is suggested so that shape function derivatives can be obtained easily in closed forms (not numerically). Because there is no mesh information, essential boundary conditions can be forced without difficulty, and interface conditions that are caused as a result of physical discontinuities would be imposed in a new and efficient manner. It is simple to program and, in comparison with the most traditional schemes of the meshless methods, is faster; however, its accuracy can be at the same level.

According to the necessary conditions that a shape function must have, in [8], a new shape function has been directly introduced without using any basis function and superfluous time-consuming process. The following function, for one-dimensional case, has continuity and partition of unity conditions, which are the essential provisions of any shape functions:

$$N(x - x_i) = N_i(x) = \frac{w_i(x)}{\sum_j w_j(x)} \tag{1}$$

where x_i is the position of the node related to the shape function, $N_i(x)$ is the shape function, and $w_i(x)$ is the weighting function. In this work, the exponential function is suggested for the weighting function as follows:

DOI: 10.1002/jnm

$$w(x-x_i) = w_i(x) = \exp(-\alpha|x-x_i|) \tag{2}$$

where α is an independent positive coefficient that can change the overhang width of the shape function, and its optimal setting increases the accuracy of the method. In each dimension, the weight function would be the same as Eq. (2), and by multiplying them, the weight function in two-dimensional and three-dimensional cases can be obtained. For example, the proposed shape function in a three-dimensional case is as follows:

$$w_i(x,y,z) = \exp(-\alpha_x|x-x_i| - \alpha_y|y-y_i| - \alpha_z|z-z_i|) \tag{3}$$

where (x_i, y_i, z_i) are coordinates of node i.

Because some of the shape functions, arisen from conventional meshless methods, do not satisfy the Kronecker delta function property [6], imposition of the essential boundary conditions is another problem in these methods. Some authors have proposed the use of the Lagrange multiplier and penalty method, among other techniques, to overcome this drawback [16]. A mixed formulation has been presented in [17], which combines Shepard shape functions for inner nodes to reduce the computational time and RPIM shape functions for boundary nodes to impose the essential boundary conditions.

It is interesting to note that in the suggested shape function, by minimizing the overhang radius of the shape function by using the correct set of α, the value of the shape function in the other nodes would be close to zero. So the boundary conditions will be enforced accurately with no trouble [18,19]. For this reason, to construct shape functions that correspond to boundary nodes (which lie on the Dirichlet boundaries), we can choose the appropriate value for α to make the overhang radius of the function small enough. This manner makes it possible to impose essential boundary conditions directly.

By choosing the exponential function as the weighting function, shape function derivatives can be obtained easily in closed forms. In [8], shape function derivatives are represented for one-dimensional and two-dimensional cases. For a three-dimensional case, shape function derivatives can be obtained as follows:

$$\frac{\partial N_i(x,y,z)}{\partial x} = \alpha_x\left[-\text{sign}(x-x_i) + \frac{s_{1x}}{s_0}\right]\cdot N_i(x,y,z) \tag{4}$$

$$\frac{\partial N_i(x,y,z)}{\partial y} = \alpha_y\left[-\text{sign}(y-y_i) + \frac{s_{1y}}{s_0}\right]\cdot N_i(x,y,z) \tag{5}$$

$$\frac{\partial N_i(x,y,z)}{\partial z} = \alpha_z\left[-\text{sign}(z-z_i) + \frac{s_{1z}}{s_0}\right]\cdot N_i(x,y,z) \tag{6}$$

$$\frac{\partial^2 N_i(x,y,z)}{\partial x^2} = 2\alpha_x \ \frac{\partial N_i(x,y,z)}{\partial x}\cdot\frac{s_{1x}}{s_0} \tag{7}$$

$$\frac{\partial^2 N_i(x,y,z)}{\partial y^2} = 2\alpha_y \ \frac{\partial N_i(x,y,z)}{\partial y}\cdot\frac{s_{1y}}{s_0} \tag{8}$$

$$\frac{\partial^2 N_i(x,y,z)}{\partial z^2} = 2\alpha_z \ \frac{\partial N_i(x,y,z)}{\partial z}\cdot\frac{s_{1z}}{s_0} \tag{9}$$

$$\begin{aligned}\frac{\partial^2 N_i}{\partial p\partial q} = {} & \alpha_p\frac{\partial N_i}{\partial q}\cdot\frac{s_{1p}}{s_0} + \alpha_q\frac{\partial N_i}{\partial p}\cdot\frac{s_{1q}}{s_0} \\ & + \alpha_p\alpha_q\cdot\left[\text{sign}(p-p_i)\cdot\text{sign}(q-q_i) - \frac{s_{1pq}}{s_0}\right]\cdot N_i\end{aligned} \tag{10}$$

where $p, q = x, y, z$ and

$$\begin{aligned} s_0 &= \textstyle\sum_i w_i(x,y,z) \\ s_{1x} &= -\textstyle\sum_i \text{sign}(x-x_i)\cdot w_i(x,y,z) \\ s_{1y} &= -\textstyle\sum_i \text{sign}(y-y_i)\cdot w_i(x,y,z) \\ s_{1z} &= -\textstyle\sum_i \text{sign}(z-z_i)\cdot w_i(x,y,z) \\ s_{1pq} &= \textstyle\sum_i \text{sign}(p-p_i)\cdot\text{sign}(q-q_i)\cdot w_i(x,y,z) \end{aligned} \tag{11}$$

and other derivatives can be obtained in the same way easily.

The proposed shape function and its derivatives possess acceptable continuity to use them for solving electromagnetic problems by using the meshless methods. The simplicity of the proposed

DOI: 10.1002/jnm

function leads to the fast obtainment of all shape functions and decreases the simulation time of the meshless method significantly in comparison with conventional meshless methods. It is due to the elimination of the computation of a large matrix inversion for obtaining shape functions' construction. In other words, in the introduced method, when the shape functions are constructed directly, there is no need to compute the matrix inversion. So in conventional meshless methods where the matrix inversion must be performed to construct shape functions by increasing the number of nodes when the dimensions of the resulted matrices are enlarged, the load of calculations would extremely increase.

3. MESHLESS FORMULATION

According to the formulation procedures, meshless methods fall into two categories: meshless methods based on collocation techniques and on weak forms.

3.1. Meshless methods based on collocation techniques

These meshless methods are called meshless collocation methods or meshless strong-form methods. In these methods, the strong forms of governing equations and equations for boundary conditions are directly discretized at the field nodes by using simple collocation techniques to obtain a set of discretized system equations [20,21]. Meshless strong-form methods have some attractive advantages: a simple algorithm, computational efficiency, and truly meshless. However, meshless strong-form methods are often unstable, not robust, and inaccurate, especially for problems with derivative boundary conditions [6].

3.2. Meshless methods based on weak forms

In meshless weak-form methods, the governing PDEs with derivative boundary conditions are first transformed to a set of the so-called weak-form integral equations. In almost all electromagnetic problems, the boundary-value problems under consideration are defined by a second-order differential equation as follows:

$$-\frac{\partial}{\partial x}\left(\beta_x \frac{\partial \varphi}{\partial x}\right) - \frac{\partial}{\partial y}\left(\beta_y \frac{\partial \varphi}{\partial y}\right) - \frac{\partial}{\partial z}\left(\beta_z \frac{\partial \varphi}{\partial z}\right) + \beta\varphi = f \ \text{ in } \ \Omega \tag{12}$$

where φ is an unknown field function; β_x, β_y, β_z, and β are known parameters or functions associated with the physical properties of the solution domain; and f is a known source or excitation function. All types of boundary conditions could be expressed as an essential (Dirichlet) boundary condition

$$\varphi = p \text{ on } \ \Gamma_1 \tag{13}$$

or as a boundary condition of the third kind

$$\left(\beta_x \frac{\partial \varphi}{\partial x}\hat{a}_x + \beta_y \frac{\partial \varphi}{\partial y}\hat{a}_y + \beta_z \frac{\partial \varphi}{\partial z}\hat{a}_z\right)\cdot n + \gamma\varphi = q \text{ on } \ \Gamma_2 \tag{14}$$

where $\Gamma(=\Gamma_1 + \Gamma_2)$ denotes the contour or enclosing of area Ω (problem domain); $\hat{n}$ is the outward normal unit vector; and γ, p, and q are known parameters. To use the variational method to formulate meshless methods, first, we need to establish the required variational principle. For the aforementioned problem, it can be shown that the solution can be obtained by solving the equivalent variational problem defined by the following:

$$\begin{cases} \delta F(\varphi) = 0 \\ \varphi = p \qquad \text{on } \ \Gamma_1 \end{cases} \tag{15}$$

where

$$\begin{aligned} F(\varphi) = \frac{1}{2}\int\int\int_{\Omega}\left[\beta_x\left(\frac{\partial \varphi}{\partial x}\right)^2 + \beta_y\left(\frac{\partial \varphi}{\partial y}\right)^2 + \beta_z\left(\frac{\partial \varphi}{\partial z}\right)^2 + \beta\varphi^2\right]\mathrm{d}\Omega \\ + \int_{\Gamma_2}\left(\frac{\gamma}{2}\varphi^2 - q\varphi\right)d\Gamma - \int\int\int \Omega f\varphi d\Omega \end{aligned} \tag{16}$$

This means that by minimizing Eq. (15) and enforcing the essential boundary condition, the unknown field function can be obtained.

DOI: 10.1002/jnm

In the meshless method, the field function ($\varphi(x)$) would be approximated as follows:

$$\varphi(\mathbf{x}) \simeq \tilde{\varphi}(\mathbf{x}) = \sum_{i=1}^{M} N_i(\mathbf{x}) \cdot a_i \tag{17}$$

where N_i is the shape function, a_i is the unknown coefficient that must be obtained, and M is the number of nodes. By substituting Eq. (17) into Eq. (16) and taking the derivative of F with respect to a_i, we obtain

$$\begin{aligned} \frac{\partial F}{\partial a_i} = \sum_{j=1}^{M} a_j \iiint_{\Omega} \left(\beta_x \frac{\partial N_i}{\partial x}\frac{\partial N_j}{\partial x} + \beta_y \frac{\partial N_i}{\partial y}\frac{\partial N_j}{\partial y} + \beta_z \frac{\partial N_i}{\partial z}\frac{\partial N_j}{\partial z} + \beta N_i N_j \right) d\Omega \\ - \iiint_{\Omega} f N_i d\Omega = 0, i = 1, 2, \ldots, M \end{aligned} \tag{18}$$

The aforementioned relation can be written in the following matrix form:

$$[K] \cdot \{a\} = \{b\} \tag{19}$$

where

$$\{a\} = [a_1, a_2, \ldots, a_M]^T \tag{20}$$

$$K_{ij} = \int\int\int_{\Omega} \left(\beta_x \frac{\partial N_i}{\partial x}\frac{\partial N_j}{\partial x} + \beta_y \frac{\partial N_i}{\partial y}\frac{\partial N_j}{\partial y} + \beta_z \frac{\partial N_i}{\partial z}\frac{\partial N_j}{lz} + \beta N_i N_j \right) d\Omega \tag{21}$$

$$b_i = \int\int\int_{\Omega} f N_i d\Omega \tag{22}$$

Note that if the shape functions satisfy the Kronecker delta function property, then coefficient a_i would be equal to the value of unknown field φ at related nodes.

One of the complications in using meshless methods is that computing these integrals in the aforementioned relations over the entire problem domain is a time-consuming step. It is evident that the proposed shape function and its derivatives have an influence domain where their values are considerable. Out of this domain, in a recognizable distance from a related node, the shape function and its derivatives have very small values nearly close to zero. By solving α_x, α_y, and α_z in Eq. (3), the damping ratio of the shape function and also the distance can be evaluated accurately. So we can employ a relaxed weak form with integration over a small local quadrature domain, that is, the influence domain. Although in the other schemes of the meshless methods, it is very difficult to evaluate the distance accurately or in some of them, such as the multiquadric RPIM, the shape function has a zero value in a far distance from a related node. Therefore, with the use of the proposed shape function in a meshless method, a lot of time can also be saved in this step.

4. NODAL INTEGRATION

In a conventional meshfree method based on weak forms, a background mesh is needed for the implementation of numerical integration. For the present nodal integration method, a background mesh is used for constructing the nodal integration domain for each node. The background mesh is not used for the shape function construction, which is constructed using a same set of nodes located in a local support domain.

Consider now an integral

$$I = \int_{\Omega} f(\mathbf{x}) d\Omega \tag{23}$$

where $f(\mathbf{x})$ is an arbitrary function integrable and Ω is the domain of the problem, which is represented by a set of M nodes distributed in the problem domain.

In a nodal integration scheme, the domain Ω is divided into a set of non-overlapping subdomain Ω_i ($i = 1,2,\ldots,M$), each of them includes a node, and $\Omega = \sum_{i=1}^{M} \Omega_i$. Then the integration, Eq. (23), can then be expressed as

DOI: 10.1002/jnm

$$I \simeq \sum_{i=1}^{M} \int_{\Omega_i} f(\mathbf{x}) d\Omega \tag{24}$$

The question now is how to evaluate $\int_{\Omega_i} f(\mathbf{x}) \mathrm{d}\Omega_i$ over the nodal integration domain Ω_i. Here, to evaluate each subdomain integral, we employ a simple and efficient approach based on the Taylor series extension [12]. The basic idea of this approach is to extend the integral function into some terms of the Taylor series, and the integration will be approximately performed on these terms. In [12], there is an excellent and complete job on one-dimensional and two-dimensional integrations. In this paper, we will do all in a three-dimensional way.

With the application of the Taylor series extension, a three-dimensional continuous function $f(x, y, z)$ can be approximated in the vicinity of point (x_0, y_0, z_0) as follows:

$$\begin{aligned} f(x,y,z) = & f(x_0,y_0,z_0) + \left(x\frac{\partial}{\partial x} + y\frac{\partial}{\partial y} + z\frac{\partial}{\partial z}\right) f(x_0,y_0,z_0) \\ & + \frac{1}{2!}\left(x\frac{\partial}{\partial x} + y\frac{\partial}{\partial y} + z\frac{\partial}{\partial z}\right)^2 f(x_0,y_0,z_0) \end{aligned} \tag{25}$$

The integration for function $f(x, y, z)$ over the nodal integration domain Ω_i can be expressed as follows:

$$\begin{aligned} \int\int\int_{\Omega_i} f(x,y,z)d\Omega \simeq & \int\int\int_{\Omega_i} \Big[f(x_i,y_i,z_i) + \left(x\frac{\partial}{\partial x} + y\frac{\partial}{\partial y} + z\frac{\partial}{\partial z}\right) f(x_i,y_i,z_i) \\ & + \frac{1}{2!}\left(x\frac{\partial}{\partial x} + y\frac{\partial}{\partial y} + z\frac{\partial}{\partial z}\right)^2 f(x_i,y_i,z_i)\Big] d\Omega \\ = & f(x_i,y_i,z_i)\int\int\int_{\Omega_i} d\Omega + f_x(x_i,y_i,z_i)\int\int\int_{\Omega_i} x d\Omega + f_y(x_i,y_i,z_i)\int\int\int_{\Omega_i} y d\Omega \\ & + f_z(x_i,y_i,z_i)\int\int\int_{\Omega_i} z d\Omega + \frac{1}{2}f_{xx}(x_i,y_i,z_i)\int\int\int_{\Omega_i} x^2 d\Omega \\ & + \frac{1}{2}f_{yy}(x_i,y_i,z_i)\int\int\int_{\Omega_i} y^2 d\Omega + \frac{1}{2}f_{zz}(x_i,y_i,z_i)\int\int\int_{\Omega_i} z^2 d\Omega \\ & + f_{xy}(x_i,y_i,z_i)\int\int\int_{\Omega_i} xy d\Omega + f_{xz}(x_i,y_i,z_i)\int\int\int_{\Omega_i} xz d\Omega \\ & + f_{yz}(x_i,y_i,z_i)\int\int\int_{\Omega_i} yz d\Omega \end{aligned} \tag{26}$$

or

$$\begin{aligned} \int\int\int_{\Omega_i} f(x,y,z)d\Omega \simeq & f(x_i,y_i,z_i)A_i + f_x(x_i,y_i,z_i)A_{xi} + f_y(x_i,y_i,z_i)A_{yi} + f_z(x_i,y_i,z_i)A_{zi} \\ & + \frac{1}{2}f_{xx}(x_i,y_i,z_i)A_{xxi} + \frac{1}{2}f_{yy}(x_i,y_i,z_i)A_{yyi} + \frac{1}{2}f_{zz}(x_i,y_i,z_i)A_{zzi} \\ & + f_{xy}(x_i,y_i,z_i)A_{xyi} + f_{xz}(x_i,y_i,z_i)A_{xzi} + f_{yz}(x_i,y_i,z_i)A_{yzi} \end{aligned} \tag{27}$$

where A_i is the area of the nodal integration domain of the ith node,

$$A_{xi} = \iiint_{\Omega_i} x d\Omega, \qquad A_{yi} = \iiint_{\Omega_i} y d\Omega, \qquad A_{zi} = \iiint_{\Omega_i} z d\Omega \tag{28}$$

are the area moments of the first order for the integration domain of the ith node, and

$$\begin{aligned} A_{xxi} &= \int\int\int_{\Omega_i} x^2 d\Omega, \qquad A_{yyi} = \int\int\int_{\Omega_i} y^2 d\Omega, \qquad A_{zzi} = \int\int\int_{\Omega_i} z^2 d\Omega \\ A_{xyi} &= \int\int\int_{\Omega_i} xy d\Omega, \qquad A_{xzi} = \int\int\int_{\Omega_i} xz d\Omega, \qquad A_{yzi} = \int\int\int_{\Omega_i} yz d\Omega \end{aligned} \tag{29}$$

are the area moments of the second order for the integration domain of the ith node.

DOI: 10.1002/jnm

To apply the nodal integration technique, a background cell is required to divide the problem domain into nodal integration domains, each of which includes a node. When the nodes are regularly distributed, a rectangular domain can be used as the nodal integration domain Ω_i, and the assembly of all the rectangles organizes the problem domain. For irregularly distributed nodes, a tessellation can always be generated automatically by connecting the centroids of the triangles and the mid-edge points [23].

According to Eq. (27), the area A_i and the moments A_{xi}, A_{yi}, A_{zi}, A_{xxi}, A_{yyi}, A_{zzi}, A_{xyi}, A_{xzi}, and A_{yzi} for the ith field node can be calculated during the pre-process stage for later use in the numerical integration, because they depend only on the geometry of the nodal integration domain.

In general, the amount of the Taylor series terms is depended on our needed accuracy. Usually, smaller influence domains need fewer terms. In practice, node influence domain in the regions with high density node distribution is small; but in these regions, fields have sharper changes, and reducing the Taylor series terms causes to increase approximation error. So, in all areas, we use the same amount of terms, which is shown in Eq. (25).

5. NUMERICAL EXPERIMENTS

5.1. Electrostatic problem

To evaluate the effectivity and the accuracy of the proposed method in electrostatic problems, a three-dimensional problem, whose analytical solution can be obtain easily, is analyzed here. Suppose a cubical box (scale size) with perfect electric conduct (PEC) walls, as shown in Figure 1. The boundary conditions are $V=10\sin(\pi x)\sin(\pi y)V$ on the top boundary and $V=0V$ to others. By considering the aforementioned condition on the top boundary, there is no need to consider that the top is separated by an infinitesimal distance that causes the analytic solution to require an infinite number of terms. So this cubical box will be a good benchmark with analytical solution for validation of the proposed meshless method. The analytical solution for this problem is given by

$$V(x,y,z)=\frac{10}{\sinh\left(\sqrt{(\pi)^2+(\pi)^2}\right)}\sin(\pi x)\sin(\pi y)\sinh\left(\sqrt{(\pi)^2+(\pi)^2}z\right) \tag{30}$$

To obtain the potential distribution by using the proposed method, the Laplace equation for potential, which can be obtained by setting $\beta_x=\beta_y=\beta_z=1$ and $\beta=f=0$ in Eq. (12), must be solved. For this,

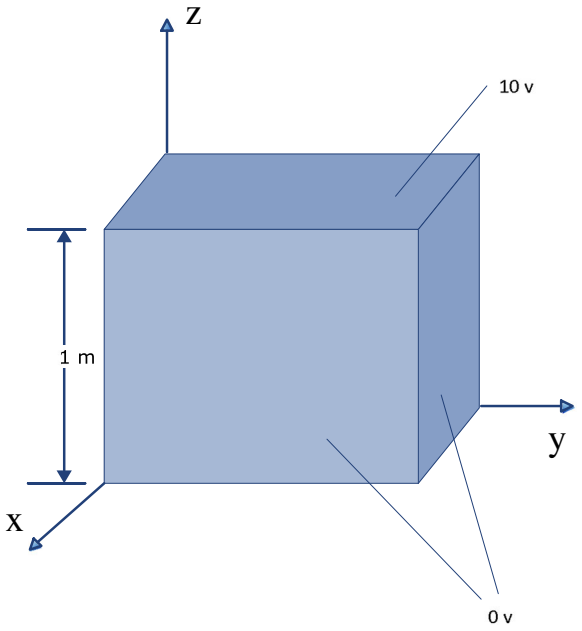

Figure 1. The electrostatic cubical box.

DOI: 10.1002/jnm

the solution domain is discretized by only $(9 \times 9 \times 9)$ regular grid of nodes, and the shape parameters are set as $\alpha_x = 10/d_x$, $\alpha_y = 10/d_y$, and $\alpha_z = 10/d_z$, where d_x, d_y, and d_z are the nodal distance in x, y, and z directions, respectively. Figure 2(a) and (b) shows the potential distributions (equipotential counters) obtained using the proposed method at $y = 0.5$ m and $z = 0.5$ m planes, respectively.

To illustrate more qualities of the proposed method as a truly meshless method, a comparison on the accuracy between the proposed method and the meshless method, which uses background mesh to compute weak-form integrals, is carried out using an error analysis with the following equation:

$$\text{Error} = \frac{1}{M} \frac{\sum_{i=1}^{M} |V - \tilde{V}|}{\sum_{i=1}^{M} |V|} \tag{31}$$

where M is the total number of nodes for solution and $\tilde{V}$ and V are the numerical and analytical solutions, respectively. Figure 3 demonstrates how solution accuracy is affected by the number of nodes. As expected, in both, as the number of nodes increases, the error in the numerical results decreases generally. Moreover, as it is seen, non-truly meshless method reaches higher accuracy, but it must be noted that we want to have a truly meshless method, although the truly meshless method has also an acceptable accuracy.

5.2. Electromagnetic problem

Although the application of the meshless formulation to electrostatic problems is straightforward, its application to electromagnetic problems is somewhat more involved. On the other hand, in most

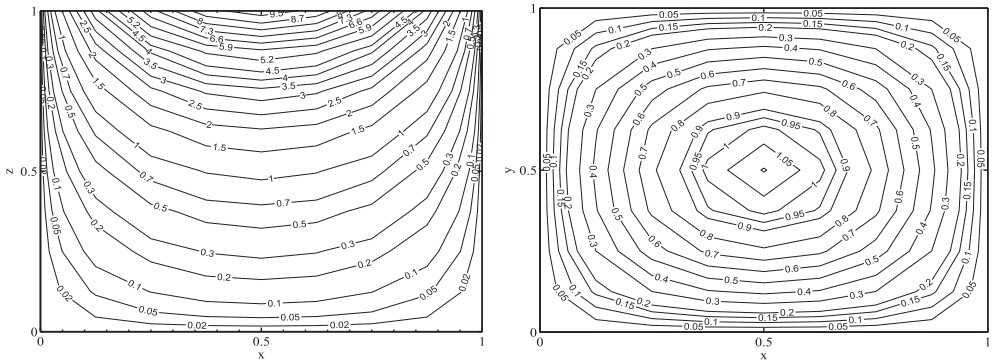

Figure 2. The equipotential counters in the cubical box at (a) $y = 0.5$ m plane and (b) $z = 0.5$ m plane.

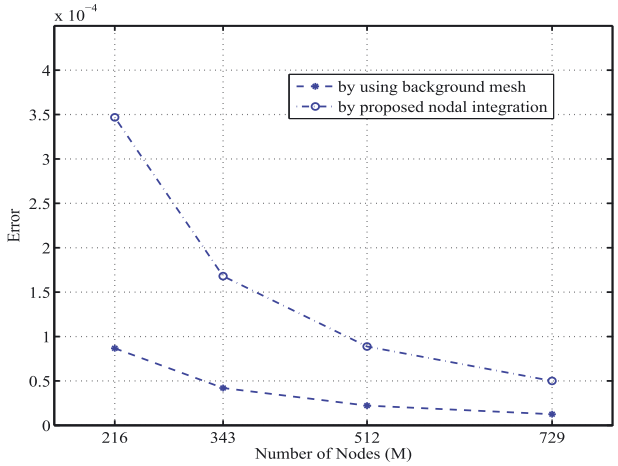

Figure 3. The relative norm error when refining the node distribution.

DOI: 10.1002/jnm

previous works, there is no comprehensive research on solving the wave equation in the frequency domain by truly meshless methods. So in this subsection, we employ the proposed meshless method to solve the wave equation in a three-dimensional infinitely air-filled rectangular waveguide in which its geometry is illustrated in Figure 4.

The electric field sought solves the following wave equation:

$$\nabla \times \left(\frac{1}{\mu_r}\nabla \times \vec{E}\right) - \varepsilon_r k_0^2 \vec{E} = 0 \tag{32}$$

where k_0 is the propagation constant. In conjunction with this,

$$E_t = 0 \text{ on conducting walls} \tag{33}$$

as the Dirichlet boundary condition on the PEC walls.

To apply the meshless method to an infinitely rectangular waveguide with an unbounded region, it first is necessary to truncate the infinite region to a finite region. This can be accomplished by placing fictitious planes on each of the front and back sides of the waveguide called S_i and S_f. So it is necessary to prescribe a boundary condition for each of these fictitious planes. For this, let us assume that the waveguide is operating at a frequency at which only the dominant mode TE_{z10} can propagate without attenuation. Further, let us assume that S_i and S_f are placed sufficiently far from each other. In [24], it has been shown that the boundary conditions on the S_i and the S_f can be considered as the third kind of boundary condition and generally be expressed in the following form:

$$\hat{n} \times \left(\nabla \times \vec{E}\right) + \kappa \hat{n} \times \left(\hat{n} \times \vec{E}\right) = \vec{U} \tag{34}$$

so that $\hat{n}$ is an outward normal unit vector on boundary, and we obtained $\kappa = jk_{z10}$ and $\vec{U} = -2jE_0 k_{z10}\sin(\pi x/a)\hat{y}$ for S_i and $\kappa = jk_{z10}$ and $U = 0$ for S_f. In this case, S_i, in addition to being a non-reflecting plane, can also be considered as an exciting surface. Moreover,

$$k_{z10} = \sqrt{k_0^2 - (\pi/a)^2} \tag{35}$$

where a is the length of the waveguide in x direction.

The equivalent variational problem for the boundary-value problem defined previously is given by

$$\begin{cases} \delta F = 0 \\ \hat{n} \times \rightarrow E = 0 \qquad \text{on the PEC walls} \end{cases} \tag{36}$$

where

$$\begin{aligned} F\left(\vec{E}\right) = \frac{1}{2}\int\int\int_v \left[\frac{1}{\mu_r}\left(\nabla \times \vec{E}\right)\cdot\left(\nabla \times \vec{E}\right) - k_0^2 \varepsilon_r \vec{E}\cdot\vec{E}\right] dv \\ + \int\int_s \left[\frac{\kappa}{2}\left(\hat{n} \times \vec{E}\right)\cdot\left(\hat{n} \times \vec{E}\right) + \vec{E}\cdot\vec{U}\right] ds \end{aligned} \tag{37}$$

and $S = S_i + S_f$.

To solve the variational problem described previously, we may first rewrite Eq. (37) in terms of the scalar components as

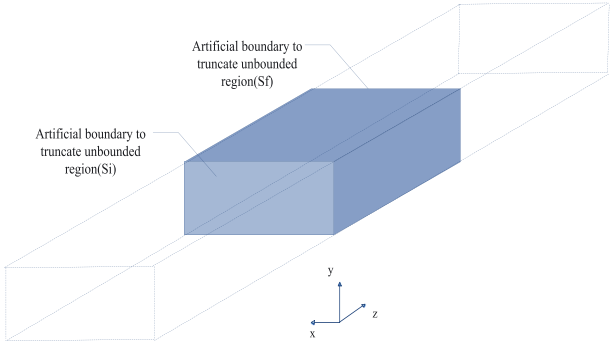

Figure 4. The rectangular waveguide and its artificial boundary condition (absorbing boundary condition).

DOI: 10.1002/jnm

$$F(\vec{E}) = \frac{1}{2}\iiint_v \left[\frac{1}{\mu_r}\left(\left(\frac{\partial E_z}{\partial y} - \frac{\partial E_y}{\partial z}\right)^2 + \left(\frac{\partial E_x}{\partial z} - \frac{\partial E_z}{\partial x}\right)^2 + \left(\frac{\partial E_y}{\partial x} - \frac{\partial E_x}{\partial y}\right)^2\right)\right.$$
$$\left. -k_0^2\varepsilon_r\left(E_x^2 + E_y^2 + E_z^2\right)\right]dv + \int\int_{s_i}\left[\frac{\kappa}{2}\left(E_x^2 + E_y^2\right) + \left(E_y \cdot U_y\right)\right]ds + \int\int_{s_f}\frac{\kappa}{2}\left(E_x^2 + E_y^2\right)ds \tag{38}$$

By substituting

$$\begin{aligned} E_x(x,y,z) &\simeq \sum_{i=1}^{M} a_i \cdot N_i(x,y,z) \\ E_y(x,y,z) &\simeq \sum_{i=1}^{M} b_i \cdot N_i(x,y,z) \\ E_z(x,y,z) &\simeq \sum_{i=1}^{M} c_i \cdot N_i(x,y,z) \end{aligned} \tag{39}$$

into Eq. (38) and taking the derivative of F with respect to a_i, b_i, and c_i, we achieve the following system, which must be solved to obtain constant coefficients:

$$[K]\cdot\begin{Bmatrix}\{a\}\\\{b\}\\\{c\}\end{Bmatrix} + \begin{bmatrix}[K^{xx,si}] & [K^{xy,si}] & [K^{xz,si}]\\ [K^{yx,si}] & [K^{yy,si}] & [K^{yz,si}]\\ [K^{zx,si}] & [K^{zy,si}] & [K^{zz,si}]\end{bmatrix}\cdot\begin{Bmatrix}\{a^{si}\}\\\{b^{si}\}\\\{c^{si}\}\end{Bmatrix}$$
$$+\begin{bmatrix}[K^{xx,sf}] & [K^{xy,sf}] & [K^{xz,sf}]\\ [K^{yx,sf}] & [K^{yy,sf}] & [K^{yz,sf}]\\ [K^{zx,sf}] & [K^{zy,sf}] & [K^{zz,sf}]\end{bmatrix}\cdot\begin{Bmatrix}\{a^{sf}\}\\\{b^{sf}\}\\\{c^{sf}\}\end{Bmatrix} = \begin{Bmatrix}\{B^{x,si}\}\\\{B^{y,si}\}\\\{B^{z,si}\}\end{Bmatrix} \tag{40}$$

where

$$[K] = \begin{bmatrix}[K^{xx}] & [K^{xy}] & [K^{xz}]\\ [K^{yx}] & [K^{yy}] & [K^{yz}]\\ [K^{zx}] & [K^{zy}] & [K^{zz}]\end{bmatrix} \tag{41}$$

and

$$K^{xx}{}_{ij} = \int\int\int_v \frac{1}{\mu_r}\left(\frac{\partial N_i}{\partial y}\cdot\frac{\partial N_j}{\partial y} + \frac{\partial N_i}{\partial z}\frac{\partial N_j}{\partial z}\right) \tag{42}$$

$$K^{yy}{}_{ij} = \int\int\int_v \frac{1}{\mu_r}\left(\frac{\partial N_i}{\partial x}\cdot\frac{\partial N_j}{\partial x} + \frac{\partial N_i}{\partial z}\frac{\partial N_j}{\partial z}\right) \tag{43}$$

$$K^{zz}{}_{ij} = \int\int\int_v \frac{1}{\mu_r}\left(\frac{\partial N_i}{\partial x}\cdot\frac{\partial N_j}{\partial x} + \frac{\partial N_i}{\partial y}\frac{\partial N_j}{\partial y}\right) \tag{44}$$

$$K^{pq}{}_{ij} = \int\int\int_v \frac{1}{\mu_r}\left(\frac{\partial N_i}{\partial q}\cdot\frac{\partial N_j}{\partial p}\right) \tag{45}$$

In Eq. (45), $p, q = x, y, z$ and $p \neq q$. To incorporate the boundary condition of the third kind, at first, we may approximate the field functions on the surface of the fictitious planes by

DOI: 10.1002/jnm

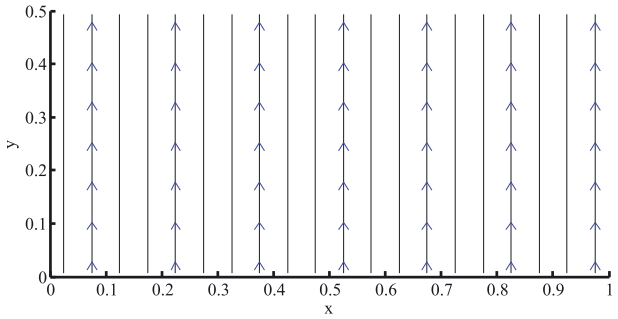

Figure 5. The analytical solution for the $\mathbf{TE_{10}}$ electric field contour at a $\mathbf{z = cte}$ plane.

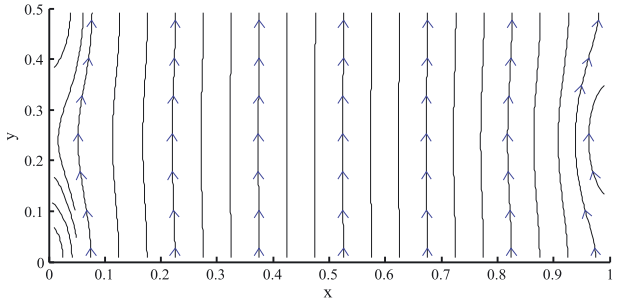

Figure 6. The computed $\mathbf{TE_{10}}$ electric field contour at a $\mathbf{z = cte}$ plane by using the proposed method.

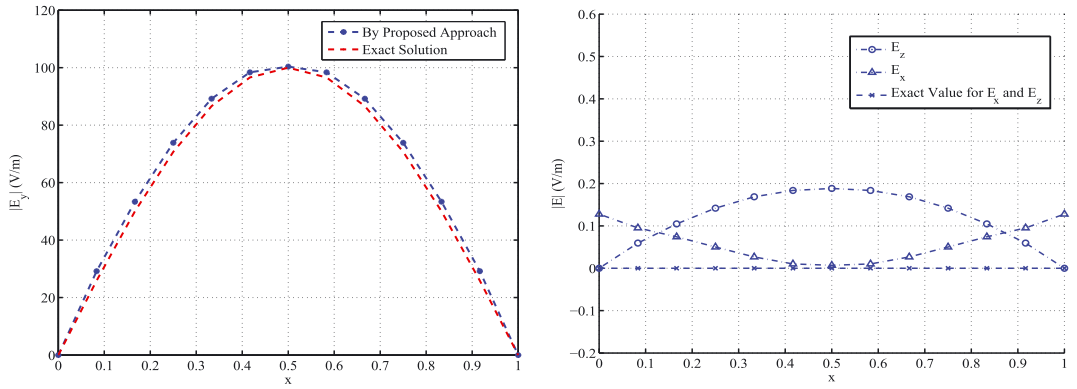

(a) (b)

Figure 7. The electric field components at a $\mathbf{z = cte}$ plane: (a) computed and exact $|\mathbf{E_y}|$ and (b) computed and exact $|\mathbf{E_x}|$ and $|\mathbf{E_z}|$.

$$
\begin{aligned}
E_x^{si}(x,y) &= \sum_{i=1}^{N_{si}} a_i^{si} N_i(x,y) \\
E_y^{si}(x,y) &= \sum_{i=1}^{N_{si}} b_i^{si} N_i(x,y) \\
E_x^{sf}(x,y) &= \sum_{i=1}^{N_{sf}} a_i^{sf} N_i(x,y) \\
E_y^{sf}(x,y) &= \sum_{i=1}^{N_{sf}} b_i^{sf} N_i(x,y)
\end{aligned}
\tag{46}
$$

where $N_i(x,y)$ is a two-dimensional shape function on the surface of the planes and N_s is the number of nodes on each fictitious plane. Moreover, a^{si}, a^{sf}, b^{si}, and b^{sf} are equal to the

DOI: 10.1002/jnm

corresponding a_i and b_i (because of the delta Kronecker property of the shape function). So we can compute the second and third integrals in Eq. (38) and incorporate them in Eq. (40) by using following matrices:

$$\begin{aligned} K^{xx,si}{}_{i,j} = K^{yy,si}{}_{i,j} = K^{xx,sf}{}_{i,j} = K^{yy,sf}{}_{i,j} = \int\int \kappa N_i(x,y) N_j(x,y) \\ K^{zz,si}{}_{i,j} = K^{xx,sf}{}_{i,j} = K^{pq,si}{}_{i,j} = K^{xx,sf}{}_{i,j} = 0 p,q = x,y,z \text{and} p \neq q \end{aligned} \tag{47}$$

and

$$B^{p,si}{}_{i} = -\int\int_{s_i} U_p \cdot N_i(x,y),\ p = x,y,z \tag{48}$$

With the use of a $(7 \times 13 \times 31)$ node distribution for the discretization of a rectangular waveguide domain (i.e., $0 < x < 1$, $0 < y < 0.5$, and $0 < z < 3$) and by setting $\alpha_x = 3/d_x$, $\alpha_y = 3/d_y$, and $\alpha_z = 3/d_z$ as the shape parameters, all coefficients for electric field components in the structure are obtained using the proposed meshless method. Figures 5 and 6 show the electric field contours calculated using an analytical approach and the proposed method at $z = 0.75$ m plane, respectively. The difference between the solutions is considerable near the vertical sides where the strength of the electric field is very close to zero in the TE_{10} mode. Moreover, Figure 7 illustrates the electric field components at the same plane separately. As expected, the TE_{10} mode is excited truthfully. As seen in Figure 7(a), the computed E_y is very similar to the exact one (i.e., $E_y = E_0 \sin(\pi x)$). Also, the computed and exact values of E_x and E_z have been illustrated in Figure 7(b). The pictures show clearly that E_x and E_z are about two orders of magnitude smaller than E_y. This means that these two components of the electric field are very close to zero in comparison with (as expected in the TE_{10} mode). Computational errors and also the used simple absorbing boundary condition made the electric field components different from their exact values slightly.

6. CONCLUSIONS

A fast truly meshless method based on a recently proposed shape function has been extended to three-dimensional electrostatic and electromagnetic problems. The used shape function is achieved directly, and its derivatives can be calculated easily in closed form. The idea of this work to reach a truly meshless method is to use the Taylor series extension to approximate fields and calculate meshless weak-form integrals without having any background mesh. At first, an electrostatic problem with an analytical solution was investigated, and then the wave propagation in a rectangular waveguide was analyzed. Absorbing the boundary condition truncated the solution domain in the waveguide. Results show that the nodal integration approach along with the new shape function and its derivatives, which are employed in this paper, can reach acceptable accuracy and that this method has no need to any background mesh. Moreover, employing the new shape function construction approach can save considerable simulation time.

REFERENCES

1. Belytschko T, Lu YY, Gu L. Element-free Galerkin method. *Int J Numer Meth Eng* 1994; **37**: 229–256.
2. Liu GR, Liu MB. *Smoothed Particle Hydrodynamics*. World Scientific Publishing Co. Ltd., Singapore, 2003.
3. Melenk JM, Babuska I. The partition of unity finite element method: basic theory and applications. *Comput Meth Appl Mech Eng* 1996; **139**:289–314.
4. Babuska I, Melenk JM. The partition of unity method. *Int J Numer Meth Eng* 1997; **40**:727–758.
5. Sibson R. A vector identity for the Dirichlet tessellation. *Math Proc Cambridge* 1980; **87**(1):151–155.
6. Liu GR, Gu YT. *An Introduction to Meshfree Methods and Their Programming*. Springer, the Netherlands 2005.
7. Razmjoo H, Movahhedi M, Hakimi A. An efficient meshless method based ona new shape function. *Int J Numer Model EL* 2010; **23**(6):503–521.
8. Razmjoo H, Movahhedi M, Hakimi A. Modification on a fast meshless method for electromagnetic field computations. *IET Sci Meas Technol* 2011; **5**(5): 175–182.
9. Razmjoo H, Movahhedi M, Hakimi A. Improved meshless method using direct shape function for computational electromagnetics. *The Asia-Pacific Microwave Conference (APMC 2010) Proceedings*, Yokohama, Japan, Dec. 2010; 2157–2160.
10. Razmjoo H, Movahhedi M, Hakimi A. Electromagnetic time domain modeling using an improved meshless method. *The International Microwave Symposium (IMS2011) Proceedings*, Baltimore, USA, Jun. 2011.
11. Beissel S, Belytschko T. Nodal integration of the element-free Galerkin method. *Comput Meth Appl Mech Eng* 1996; **139**:49–74.

DOI: 10.1002/jnm

12. Liu GR, Zhang GY, Wang YY, Zhong ZH, Li GY, Han X. A nodal integration technique for meshfree radial point interpolation method (NI-RPIM). *Int J Numer Meth Eng* 2007; **46**:341–385.
13. Chen JS, Wu CT, Yoon S, You Y. A stabilized conforming nodal integration for Galerkin mesh-free methods. *Int J Numer Meth Eng* 2001; **50**:435–66.
14. Rosca VE, Leitao VMA. Quasi-Monte Carlo mesh-free integration for meshless weak formulations. *Eng Anal Bound Elem* 2008; **32**:471–479.
15. Nagashima T. Node-by-node meshless approach and its applications to structural analysis. *Int J Numer Meth Eng* 1999; **46**:341–385.
16. Liu GR. *Mesh Free Methods: Moving beyond the Finite Element Method*. CRC Press: Boca Raton, FL, 2002.
17. Fonseca AR, Corra BC, Silva EJ, Mesquita RC. Improving the mixed formulation for meshless local Petrov–Galerkin method. *IEEE Trans Magn* 2010; **46**(8):2907–2910.
18. Hkrault C, Markcha Y. Boundary and interface conditions in meshless methods. *IEEE Trans Magn* 1999; **35**(3):1450–1453.
19. Fonseca AR, Viana SA, Silva EJ, Mesquita RC. Imposing boundary conditions in the meshless local Petrov–Galerkin Method. *IET Sci Meas Technol* 2008; **2**(6):387–394.
20. Kansa EJ. Multiquadrics—a scattered data approximation scheme with applications to computational fluid dynamics, *Comput Math Appl* 1990; **19**:127–145.
21. Liu X, Liu GR, Tai K, Gu YT, Lam KY. Polynomial point interpolation collocation method for the solution of partial differential equations. *Eng Anal Bound Elem* 2006; **30**(7):598–609.
22. Ferziger JH, Peric M. *Computational Methods for Fluid Dynamics*. Springer: Berlin, Germany, 1999.
23. Jin J-M. *The Finite Element Method in Electromagnetics*. Wiley: New York, 1993.

AUTHORS' BIOGRAPHIES

Hooman Razmjoo was born in Shiraz, Iran, on September 6, 1986. He received his BSc and MSc degrees in electrical engineering from Shahid Bahonar University of Kerman, Kerman, Iran, in 2008 and 2011. He is currently working toward a PhD degree in the Department of Electrical and Computer Engineering at Shiraz University, Shiraz, Iran. His research interests include computational electromagnetics, high-frequency circuit simulation, high-frequency microwave sources, and RF circuit design.

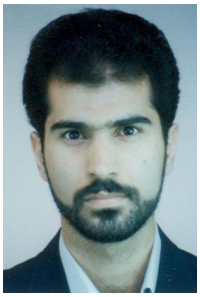

Masoud Movahhedi was born in Yazd, Iran, in 1976. He received his BSc degree from Sharif University of Technology, Tehran, Iran, in 1998 and his MSc and PhD degrees from Amirkabir University of Technology (Tehran Polytechnic), Tehran, Iran, in 2000 and 2007, all in electrical engineering. From December 2005 to September 2006, he was with the Institute for Microelectronics, Technische Universitat Wien, Austria, as a visiting student. He is currently an assistant professor at the Electrical Engineering Department, Shahid Bahonar University of Kerman, Kerman, Iran. His research interests are in the areas of computer-aided design of microwave-integrated circuits, computational electromagnetic, semiconductor high-frequency RF modeling, and metamaterials simulation. Dr Movahhedi was a recipient of the GAAS-05 Fellowship granted by the GAAS Association to young graduate researchers for his paper presented at the GAAS2005. He was also a recipient of the Electrical Engineering Department Outstanding Student Award in 2005 and 2006.

Ahmad Hakimi was born in Rafsanjan, Iran, in 1961. He received his BSc degree in electrical engineering from Technical College of Shahid Bahonar University of Kerman, Kerman, Iran, in 1986. Using the scholarship granted by the Ministry of Higher Education of Iran and Istanbul Technical University (ITU) in 1987, he has been studying for his MSc and PhD degrees in the Faculty of Electrical and Electronic Engineering at the ITU. He received his MSc and PhD degrees from ITU in 1996 and 1995 in the field of high-frequency electronics. His research interests include design and analysis of nonlinear RF circuits, numerical analysis and advanced engineering mathematics, analog filter design, and linear integrated circuits. He is currently with the Scientific and Industrial Research Center, Kerman, Iran, and the Department of Electrical Engineering, Shahid Bahonar University of Kerman, Kerman, Iran.

DOI: 10.1002/jnm